Lateral Response Evaluation of Single Piles Using Inclinometer Data

San-Shyan Lin[1] and Jen-Cheng Liao[2]

Abstract: In an effort to develop an efficient method for interpretation of lateral pile load test results via measured inclinometer data only, an analytical model is proposed based on energy conservation of a pile-soil system. A Fourier series function is used to represent deflection behavior of the pile-soil system. In order to obtain shear, moment, and soil reaction along the pile shaft, convergence of the series after differentiation is guaranteed by applying the Cesaro sum technique. The concrete cracking effect is also incorporated into the pile model to account for yielding of the pile itself. Three full-scale pile load cases are then used to verify the feasibility of the developed methodology as well as make comparison to other methods.

DOI: 10.1061/(ASCE)1090-0241(2006)132:12(1566)

CE Database subject headings: Lateral loads; Cracking; Concrete piles; Data analysis; Evaluation.

Introduction

Use of piles to resist lateral loading has attracted a lot of attention from geotechnical engineers in the past decade. However, the response of a laterally loaded pile is a complicated soil–structure interaction problem. For concrete piles, an added difficulty is the nonlinear behavior of concrete near structural failure. The lateral load behavior of single piles is often obtained via in-situ lateral pile load tests. In general, if detailed information involving *p-y* curve parameters is required, many strain gauges are often installed along the length of pile shaft to develop the bending moment versus depth relationship (Pinto et al. 1999). In this paper, the use of inclinometers is recommended for lateral pile load tests in order to obtain more detailed information for back-calculating *p-y* curves. The use of slope inclinometers to measure lateral deflection of the pile has some advantages compared to the strain gauges, which are easily damaged during pile installation or by improper handling. Additionally, inclinometer measurements are less costly compared to other alternatives. However, inclinometer data are prone to reduction errors because the slope distribution must be differentiated three times in order to obtain *p-y* curves (Brown et al. (1994); Pinto et al. 1999).

Brown et al. (1994) proposed a method for interpreting lateral load tests. The method utilizes a least-squares regression technique that will converge to a solution for analytical *p-y* curves that produce minimum error between the predicted and measured deflection versus depth profile over a range of loading. However, the analysis requires use of a computer code, COM624 (Wang and Reese 1991), to predict deflection. In addition, the shape of the *p-y* curve must be assumed and iteration over two or more soil parameters are needed for calibration of *p-y* curves. A method that needs iteration on a single parameter, the modulus of lateral soil reaction, was proposed by Pinto et al. (1999). However, this method assumes that the initial slope of the *p-y* curve increases linearly with depth, which in general can only be used for uniform sands.

A new method is proposed in this paper in an effort to develop a simple yet accurate method for interpreting lateral single-pile load test results based only on measured inclinometer data. The pile–soil interaction response is idealized as a beam on a Winkler spring medium. Fourier series functions are used as the deflection function of the pile–soil system. Although application of the Fourier series in structural mechanics problems such as beams or plates is generally used for buckling or free-vibration analyses, applications to stress analyses have also been provided by Chen et al. (1996) and Wang and Lin (1999). In order to derive the slope, shear, moment, and soil reaction of the pile, convergence of the series after differentiation is guaranteed by applying the Cesaro sum technique (Hardy 1949). Additionally, consideration of the nonlinear behavior of the reinforced concrete piles is included in the proposed method. In this paper, the authors first present the theory and development of the proposed method. Results from three full-scale pile load cases are then used to demonstrate application of the developed methodology and make comparison to other methods.

Theory

In the following sections, the deflection function of laterally loaded piles is derived based on the principal of conservation of energy and the application of the calculus of variation. Measured inclinometer data from lateral pile load tests, which implicitly

[1]Professor, Dept. of Harbor and River Engineering, National Taiwan Ocean Univ., Keelung 20224, Taiwan (corresponding author). E-mail: sslin@mail.edu.tw

[2]Post-doctoral Student, Dept. of Harbor and River Engineering, National Taiwan Ocean Univ., Keelung 20224, Taiwan.

Note. Discussion open until May 1, 2007. Separate discussions must be submitted for individual papers. To extend the closing date by one month, a written request must be filed with the ASCE Managing Editor. The manuscript for this paper was submitted for review and possible publication on August 24, 2004; approved on June 7, 2006. This paper is part of the ***Journal of Geotechnical and Geoenvironmental Engineering***, Vol. 132, No. 12, December 1, 2006. ©ASCE, ISSN 1090-0241/2006/12-1566–1573/$25.00.

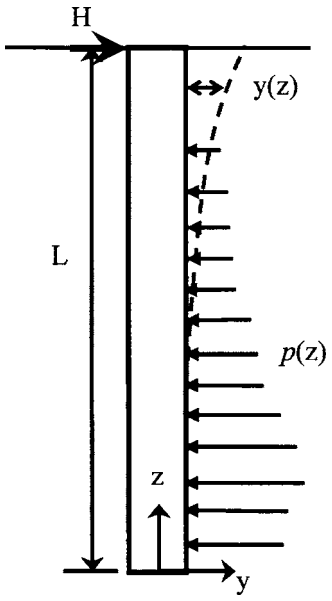

Fig. 1. Schematic diagram of soil–pile system

include pile–soil interaction effects, were utilized to determine the coefficients of the derived deflection function. Once the deflection function is established, bending moment, shear force, and p-y curves at various depths along the pile can be reduced by differentiating the deflection function. Assumptions of the derivation are:

1. Soil response is idealized as one-dimensional;
2. Pile material behavior is assumed as nonlinear elastic; and
3. Lateral loading is applied only at pile head.

Energy Method

The total energy (Π) for a pile embedded in a soil medium is given as

$$\Pi = U + V \tag{1}$$

where U=strain energy stored in the pile; and V=potential energy of soil–pile system caused by external loads.

As shown in Fig. 1, the strain energy of the pile can be expressed as (Han and Frost 2000)

$$U = \frac{1}{2}\int_0^L EI(y'')^2 dz \tag{2}$$

where E=elastic modulus of the pile; I=moment of inertia of the pile; y=lateral deflection of the pile; and z=depth along the pile shaft.

The potential energy of the soil–pile system caused by external loading applied instantaneously can be expressed as (Han and Frost 2000)

$$V = \frac{1}{2}\int_0^L p(z)ydz - Hy(L) \tag{3}$$

where $p(z)$=soil reaction at depth z; H=lateral forces applied at the pile head; $y(L)$=pile deflection at the pile head; and L=embedded length of the pile.

Substituting Eq. (2) and (3) into Eq. (1), the total potential energy of the soil–pile system can be presented as (Han and Frost 2000)

$$\Pi = \frac{1}{2}\int_0^L EI(y'')^2 dz + \frac{1}{2}\int_0^L p(z)ydz - Hy(L) \tag{4}$$

Subsequently, by applying the calculus of variations to Eq. (4), the following Euler-Lagrangian governing equation for the pile–soil system can be obtained (Han and Frost 2000)

$$EIy^{IV} + p(z) = 0 \tag{5}$$

Deflection Functions

Two different boundary conditions of long piles are considered as shown in Fig. 2. The analysis presented in the following only applies to long piles. A long pile is defined with the ratio of the pile length versus the relative stiffness factor (pile stiffness/coefficient of subgrade reaction)$^{0.2}$, larger than 4 (Prakash and Sharma 1990). The first case (case I) considers the free head and fixed toe condition, which represents long piles without caps (case I). The other case (case II) considers fixed with sway at head and fixed at toe condition, which represents long piles constrained with caps at the pile head.

By applying the Rayleigh-Ritz method, the general form of the deflection that satisfies Eq. (5) can be determined by the following Fourier series as

$$y(z) = \sum_{i=1}^{n} B_i(1 - \cos \bar{N}\pi z) \tag{6}$$

where $\bar{N}=2i-1/2L$ and $\bar{N}=i/L$ represent the boundary conditions of case I and case II, respectively. Coefficients B_i can be determined by substituting Eq. (6) into Eq. (4) and minimizing the function ($\partial\Pi/\partial B_i=0$).

Alternatively expanding Eq. (6), computed deflection $\mathbf{Y_c}$ at depth z can be presented as Eq. (7)

$$\mathbf{Y_c} = \mathbf{A} \cdot \mathbf{B} \tag{7}$$

where

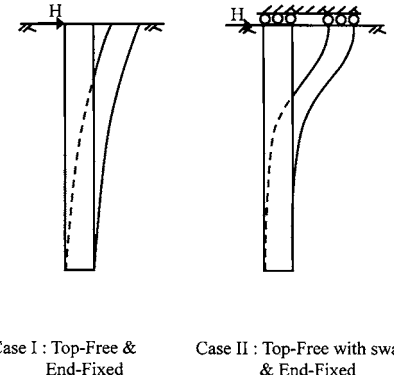

Fig. 2. Boundary conditions considered in the paper

$$\mathbf{A}_{j\times n}=\begin{bmatrix}(1-\cos \bar{N}_n\pi\cdot z_1) & \cdots & (1-\cos \bar{N}_2\pi\cdot z_1) & (1-\cos \bar{N}_1\pi\cdot z_1)\\ (1-\cos \bar{N}_n\pi\cdot z_2) & \cdots & (1-\cos \bar{N}_2\pi\cdot z_2) & (1-\cos \bar{N}_1\pi\cdot z_2)\\ . & \cdots & . & .\\ (1-\cos \bar{N}_n\pi\cdot z_j) & \cdots & (1-\cos \bar{N}_2\pi\cdot z_j) & (1-\cos \bar{N}_1\pi\cdot z_j)\end{bmatrix}$$

and

$$\mathbf{B}_{n\times 1}=\begin{Bmatrix}B_n\\ .\\ B_2\\ B_1\end{Bmatrix}$$

The least-squares rule is then applied to perform regression to solve $\mathbf{B}_{n\times 1}$ using procedures described below:

1. Obtain the square summation of the error, $\mathbf{S}$, between calculated and measured deflection, $\mathbf{Y_m}$ [Eq. (8)]

$$\mathbf{S}=(\mathbf{A}\cdot\mathbf{B}-\mathbf{Y_m})^T(\mathbf{A}\cdot\mathbf{B}-\mathbf{Y_m}) \tag{8}$$

2. For minimum error, Eq. (8) has to be applied and used to solve $\mathbf{B}_{n\times 1}$ for say, $\mathbf{Y_m}$ optimized values of coefficients B_n

$$\frac{\partial \mathbf{S}}{\partial \mathbf{B}}=2\mathbf{A}^T\cdot\mathbf{A}\cdot\mathbf{B}-2\mathbf{A}^T\cdot\mathbf{Y_m}=\mathbf{0} \tag{9}$$

Based on Euler's beam theory, once the pile deflection function is determined, the moment $M(z)$, the shear force $V(z)$, and the soil reaction $p(z)$ of the pile along the shaft can easily be obtained as given in the following equations

$$M(z)=EI\frac{d^2y(z)}{dz^2} \tag{10}$$

$$Y(z)=\frac{dM}{dz} \tag{11}$$

$$p(z)=\frac{dV}{dz} \tag{12}$$

Nonlinear Behaviors of the Piles

Reinforced concrete piles exhibit nonlinear behavior under load. Consideration of this nonlinear behavior is important to interpret the test results correctly. Based on the ACI code (1995), Reese and Van Impe (2001), and Ooi and Ramsey (2003), the effective elastic modulus of a reinforced concrete pile (E_p) can be expressed as

$$E_p=\left[1+(n-1)\frac{A_s}{A_c}\right]E_c \tag{13}$$

in which $n=E_s/E_c$; E_s=elastic modulus of the steel; E_c=elastic modulus of the concrete and is equal to $15{,}000\sqrt{f'_c}$ (kg/cm^2) (ACI 1995); A_s=area of the steel; A_c=area of concrete; and f'_c=compressive strength of the concrete.

Based on the parallel-axis theorem, moment of inertia (I_p) for the pile shaft cross sections can be expressed as (Reese and Van Impe 2001)

$$I_p=\frac{\pi}{4}r_c^4+\frac{1}{2}(n-1)A_sr_s^2 \tag{14}$$

where r_c=radius of the pile shaft; and r_s=distance from centroidal axis of gross section to centroidal axis of steel rebar.

Cracking of concrete will reduce the moment of inertia of the pile shaft. Applying the effective moment of inertia concept in ACI (1995), when the moment $M<M_{cr}$, the effective moment of inertia is

$$I_e=I_p \tag{15}$$

or when $M_{cr}<M<M_u$, the effective moment of inertia (I_e) is

$$I_e=\left(\frac{M_{cr}}{M_a}\right)^3I_g+\left[1-\left(\frac{M_{cr}}{M_a}\right)^3\right]I_{cr} \tag{16}$$

where M_a=local maximum moment along the pile shaft; $M_{cr}=f_rI_g/y_t$=cracking moment; M_u=ultimate moment; $f_r=2\sqrt{f'_c}$=tensile strength of the concrete; I_g=moment of inertia of gross concrete section about central axis; y_t=distance from centroidal axis of gross section to extreme fiber in tension; and I_{cr}=moment of inertia of cracked transformed concrete section.

The local pile bending moment can be estimated using curvature, deduced from measured displacement from inclinometer, and from pile flexural rigidity, EI. Depending on whether pile section is cracked or uncracked, I is the gross moment of inertia I_g for uncracked sections; and I is the effective moment of inertia I_c for cracked section.

Regularization with Cesaro Sum Technique

Since the deflection functions of the pile–soil system given in Eq. (6) are Fourier series functions, these functions will cause ill-posed conditions after differentiation. The Cesaro sum technique is used to guarantee the convergence of these Fourier series functions.

The general (C,r) Cesaro sum is defined as (Hardy 1949)

$$S_n=(C,r)\left(\sum_{i=0}^{n}a_i\right)\equiv\frac{C_{r-1}^{n+r-1}s_0+C_{r-1}^{n+r-2}s_1+\ \ldots\ +C_{r-1}^{r}s_{n-1}+C_{r-1}^{r-1}s_n}{C_r^{n+r}} \tag{17}$$

where $C_r^n=n!/[r!(n-r)!]$, and the partial sum is $s_i=\Sigma_{i=0}^{n}a_i(z)$, where $a_i(z)=B_i(1-\cos \bar{N}\pi z)$.

For computational convenience, the s_i terms are changed to a_i terms, and can be changed to the conventional Cesaro sum as

$$S_n=(C,1)\left(\sum_{i=0}^{n}a_i\right)\equiv\frac{s_0+s_1\ \ldots\ +s_{n-1}+s_n}{n+1} \tag{18}$$

$$(C,1)\sum_{i=0}^{n}a_i\equiv\frac{1}{n+1}\sum_{i=0}^{n}(n-i+1)a_i \tag{19}$$

Similarly, the Cesaro sum of $(C,2)$, $(C,3)$, and $(C,4)$ is

$$S_n = (C,2)\left(\sum_{i=0}^{n} a_i\right) \equiv \frac{1}{(n+1)(n+2)}\sum_{i=0}^{n}(n-i+1)(n-i+2)a_i \tag{20}$$

$$S_n = (C,3)\left(\sum_{i=0}^{n} a_i\right) \equiv \frac{1}{(n+1)(n+2)(n+3)}\sum_{i=0}^{n}(n-i+1) \times (n-i+2)(n-i+3)a_i \tag{21}$$

$$S_n = (C,4)\left(\sum_{i=0}^{n} a_i\right) \equiv \frac{1}{(n+1)(n+2)(n+3)(n+4)}\sum_{i=0}^{n}(n-i+1) \times (n-i+2)(n-i+3)(n-i+4)a_i \tag{22}$$

Or for general integer order r, the Cesaro sum can be expressed as

$$S_n = (C,r)\left(\sum_{i=0}^{n} a_i\right) \equiv \sum_{i=0}^{n}\frac{(n)\,!\,(n+i-n)!}{(n+i)\,!\,(n+r)!}a_i \tag{23}$$

Based on this regularization technique, the series representations for displacement $y(z)$, slope $\theta(z)$, moment $m(z)$, shear force $v(z)$, and soil reaction $p(z)$ are expressed in the sense of the Cesaro sum as

$$y(z) = (C,1)\left[\sum_{i=1}^{n} B_i(1-\cos\bar{N}\pi z)\right] \tag{24}$$

$$\theta(z) = y'(z) = (C,2)\left[\sum_{i=1}^{n} B_i\cdot\bar{N}\cdot(\sin\bar{N}\pi z)\right] \tag{25}$$

$$M(z) = EIy''(z) = (C,3)\left[\sum_{i=1}^{n} EI\cdot B_i\cdot\bar{N}^2\cdot(\cos\bar{N}\pi z)\right] \tag{26}$$

$$V(Z) = EIy'''(z) = (C,4)\left[\sum_{i=1}^{n} EI\cdot B_i\cdot\bar{N}^3\cdot(-\sin\bar{N}\pi z)\right] \tag{27}$$

$$p(z) = EIy''''(z) = (C,5)\left[\sum_{i=1}^{n} EI\cdot B_i\cdot\bar{N}^4\cdot(-\cos\bar{N}\pi z)\right] \tag{28}$$

in which $\bar{N}=2i-1/2L$ and $\bar{N}=i/L$ are for the boundary conditions case I and case II, respectively.

Numerical Procedures

1. Apply the boundary conditions of the pile and then compute the pile–soil deflection function from Eq. (6);
2. Substitute inclinometer measurement data into Eq. (8) and then determine **B** from Eq. (9);
3. Use the deflection function obtained from procedure 2 and utilize the Cesaro sum technique in Eqs. (26)–(28) to obtain the moment, shear, and soil reaction along pile shaft;
4. Depending on the local bending moment, update flexural rigidity at each depth of the pile; and
5. Use Eqs. (24) and (28) to obtain the p-y curves.

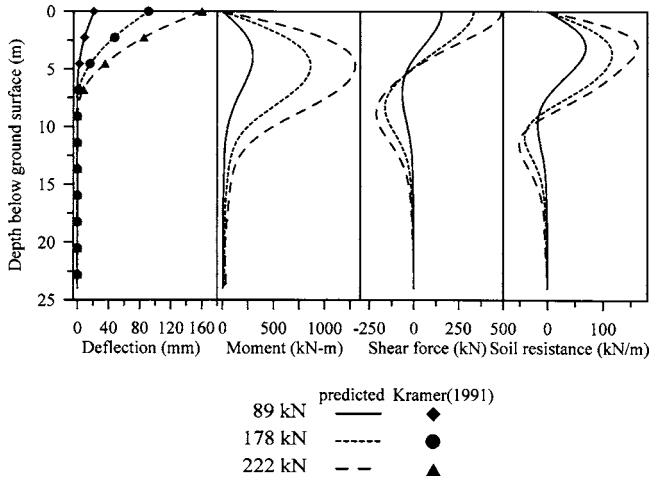

Fig. 3. Deflection, bending moment, shear force, and soil resistance distributions along the pile shaft of WDOT test pile

Examples

The use of the technique described above is illustrated using three real examples from field load tests and compared to the results obtained using other methods.

Washington DOT Lateral Pile Load Test

A full-scale lateral load test of pipe piles was conducted by Washington DOT and was reported by Kramer (1991). The 24-m-long pile, with diameter $D=0.476$ m, was embedded into deep deposit of soft clay and was subjected to lateral load with magnitude 45, 85, 178, and 222 kN applied at head. Case I boundary condition and constant EI through entire pile length are assumed to perform analysis.

Given the boundary conditions of the pile, we can fit the deflection function [Eq. (24)] to the measured inclinometer data at the loading magnitude of 222 kN as shown in Fig. 3. Subsequently, we substitute inclinometer measurement data into Eq. (8) and then determine **B** from Eq. (9). The best fit function of this case is then obtained and is expressed in the following form:

Table 1. Coefficients B_i of Washington DOT Lateral Pile Load Test (Loading Magnitude=222 kN)

Coefficients B_i	Value	Coefficients B_i	Value
B_1	1.98×10^{-1}	B_6	-2.52×10^{-4}
B_2	-5.30×10^{-2}	B_7	4.32×10^{-4}
B_3	1.99×10^{-2}	B_8	-5.81×10^{-4}
B_4	-6.43×10^{-3}	B_9	5.44×10^{-4}
B_5	1.43×10^{-3}	B_{10}	-3.61×10^{-4}

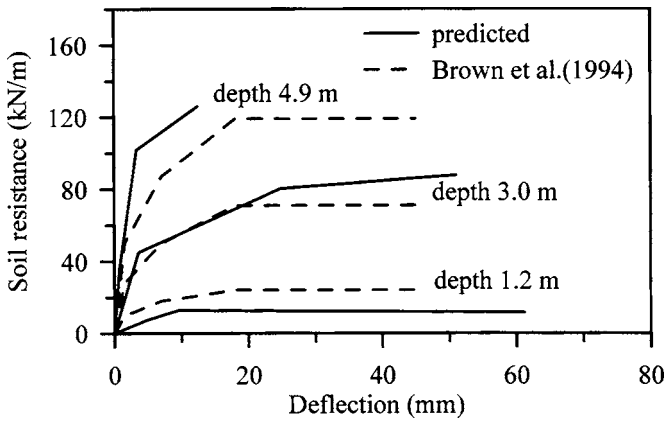

Fig. 4. *p-y* curves of WDOT test pile

$$y(z)=\left(\frac{10}{10}\right)B_1\left(1-\cos\frac{1}{2L}\pi z\right)+\left(\frac{9}{10}\right)B_2\left(1-\cos\frac{3}{2L}\pi z\right)+\left(\frac{8}{10}\right)B_3\left(1-\cos\frac{5}{2L}\pi z\right)+\left(\frac{7}{10}\right)B_4\left(1-\cos\frac{7}{2L}\pi z\right)+\left(\frac{6}{10}\right)B_5\left(1-\cos\frac{9}{2L}\pi z\right)+\left(\frac{5}{10}\right)B_6\left(1-\cos\frac{11}{2L}\pi z\right)+\left(\frac{4}{10}\right)B_7\left(1-\cos\frac{13}{2L}\pi z\right)+\left(\frac{3}{10}\right)B_8\left(1-\cos\frac{15}{2L}\pi z\right)+\left(\frac{2}{10}\right)B_9\left(1-\cos\frac{17}{2L}\pi z\right)+\left(\frac{1}{10}\right)B_{10}\left(1-\cos\frac{19}{2L}\pi z\right)$$

where the B_i ($i=1$ to 10) are given in Table. 1. Applying Eq. (25), the first derivative of the deflection function is given as

$$y'(z)=\left(\frac{10\times10}{10\times11}\right)\times\frac{\pi}{2L}B_1\left(\sin\frac{1}{2L}\pi z\right)+\left(\frac{9\times10}{10\times11}\right)\times\frac{3\pi}{2L}B_2\left(\sin\frac{3}{2L}\pi z\right)+\left(\frac{8\times9}{10\times11}\right)\times\frac{5\pi}{2L}B_3\left(\sin\frac{5}{2L}\pi z\right)+\left(\frac{7\times8}{10\times11}\right)\times\frac{7\pi}{2L}B_4\left(\sin\frac{7}{2L}\pi z\right)+\left(\frac{6\times7}{10\times11}\right)\times\frac{9\pi}{2L}B_5\left(\sin\frac{9}{2L}\pi z\right)+\left(\frac{5\times6}{10\times11}\right)\times\frac{11\pi}{2L}B_6\left(\sin\frac{11}{2L}\pi z\right)+\left(\frac{4\times5}{10\times11}\right)\times\frac{13\pi}{2L}B_7\left(\sin\frac{13}{2L}\pi z\right)+\left(\frac{3\times4}{10\times11}\right)\times\frac{15\pi}{2L}B_8\left(\sin\frac{15}{2L}\pi z\right)+\left(\frac{2\times3}{10\times11}\right)\times\frac{17\pi}{2L}B_9\left(\sin\frac{17}{2L}\pi z\right)+\left(\frac{1\times2}{10\times11}\right)\times\frac{19\pi}{2L}B_{10}\left(\sin\frac{19}{2L}\pi z\right)$$

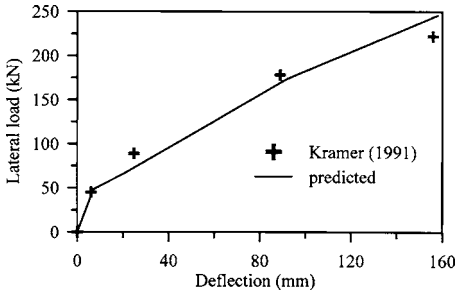

Fig. 5. Lateral load versus pile head deflection of WDOT case

Following similar procedures, the convergent solutions for the third and fourth derivative of the function can be obtained similarly by selecting different Cesaro orders.

Giving the pile flexural rigidity at each depth of the pile and utilizing the Cesaro sum technique in Eq. (26)–(28), the moment, shear, and soil reaction along the pile shaft can then be determined. Fig. 3 shows the variations of deflection, bending moment, shear force, and soil resistance distributions along the pile shaft from either analytical results or instrumentation measurement. From Fig. 3, the maximum bending moment was found at 5 m below ground surface and the corresponding shear force is zero. Fig. 4 shows the *p-y* curves obtained from the proposed method and from Brown et al. (1994) at three different depths for comparison. Reasonable agreement between two results was found. Good agreement between the predicted and measured load-deflection relationship at the pile head is also given in Fig. 5.

Lateral Shafts Test of the High Speed Rail Project in Taiwan

For the purpose of optimizing the design of pile foundations for the high speed rail system, full-scale load tests were conducted on two pile groups in Chiayi, Taiwan, in 1997 (Chen 1997). In addition to lateral load tests on the two pile groups, lateral load tests were also conducted on single piles B2 (bored pile) and P13 (precast concrete pile), by loading the piles against the adjacent pile caps. Only lateral pile test results of the single piles B2 and

Table 2. Soil Properties of the Test Site at Chiayi of the High–Speed Rail Project, Taiwan

Layer	Depth (m)	SPT-N	Classification	Description
1	0–3	1∼5	ML/SM	Fine sandy silt, yellowish brown, loose with some clayey silt.
2	3–8	8∼19	SM	Silty fine sand, gray, medium dense, occasionally with sandy silt layers.
3	8–12	4∼12	CL	Silty clay, grayish brown, medium stiff, occasionally with coarse sand seams.
4	12–16	15∼29	SM	Silty fine sand, gray, loose with fine sandy silt layer.
5	16–22	11∼23	CL/SM	Clayey silts, gray, medium dense with little sandy silts.
6	22–32	9∼27	CL	Silty clay, gray, very stiff with little fine sand.
7	32–40	14∼45	SM	Silty clay, gray, very stiff with silty fine sand layer.

Table 3. Structure Properties of Test Piles

Item	Bored pile (B2)	PC pile (P13)
Pile diameter (mm)	1,500	Precast 800 outside, 560 inside with concrete infill
Pile length (m)	34.9	34.0
Cross-sectional area (cm^2)	17,672	Solid: 5,027 Hollow: 2,564
Concrete compressive strength, f'_c (MPa)	27.47	Precast: 78.48 Infill: 20.6
Reinforcement Yield stress, f_y (MPa)	471	Precast: 1,226.25 Infill: 471

P13 are studied in this paper. Structural properties of the tested piles and typical soil properties at the test site are given in Tables 2 and 3, respectively.

Case I for boundary conditions of the free-head case was assumed for the single-bored pile B2 and PC pile P13. Derived deflection, moment, shear, and soil resistance along the pile shaft versus embedded depth for pile B2 are shown in Fig. 6. Numerical studies using the computer program LPILE (Reese et al. 2000) are also conducted using the material properties provided in Tables 2 and 3. These material properties were used as input data in the LPILE program. Reasonable agreement for the results obtained from the proposed method and from the computer program LPILE is found in the figure. It is worth pointing out that the measured inclinometer data is the only information needed in the proposed method. In addition, the pile deflection computed with

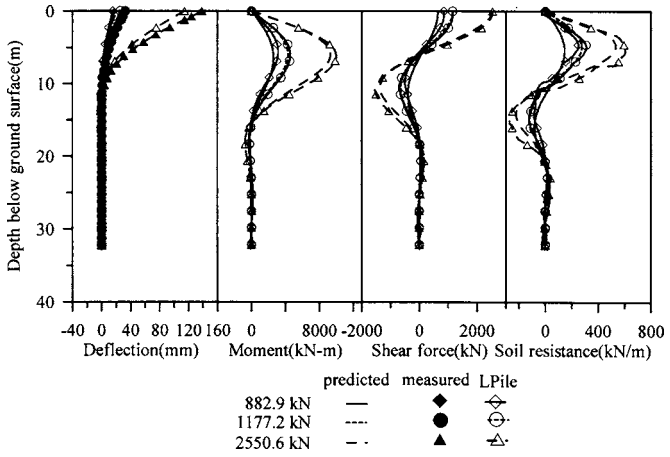

Fig. 6. Deflection, bending moment, shear force, and soil resistance distributions along the pile shaft of single-bored pile B2

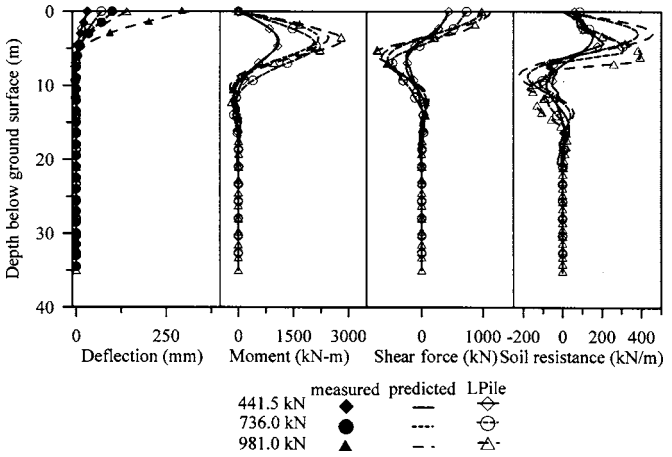

Fig. 9. Deflection, bending moment, shear force, and soil resistance distributions along the pile shaft of single PC pile P13

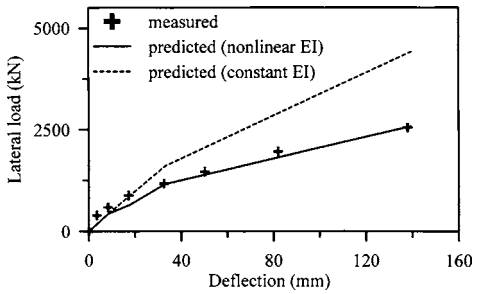

Fig. 7. Lateral load versus pile head deflection of single-bored pile B2

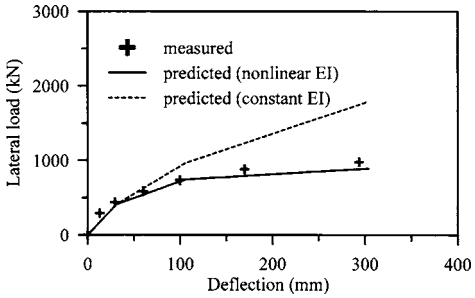

Fig. 10. Lateral load versus pile head deflection of single PC pile P13

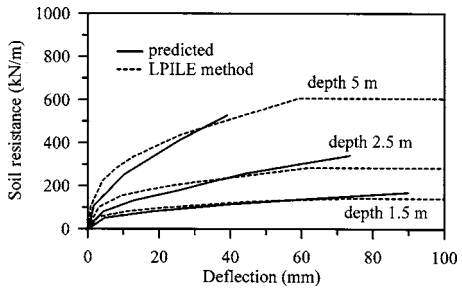

Fig. 8. *p-y* curves of single bored pile B2

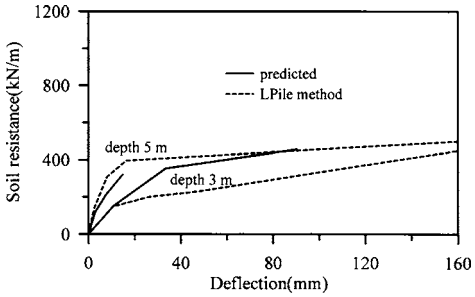

Fig. 11. *p-y* curves of single PC pile P13

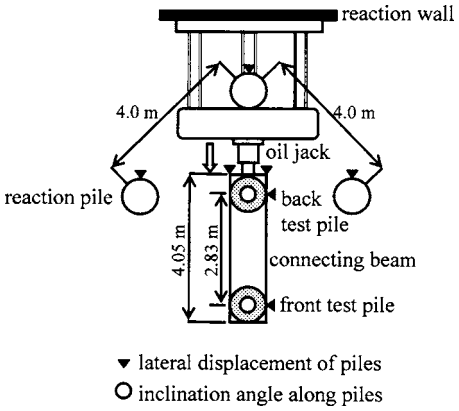

Fig. 12. Arrangement of Osaka Bay test site (adapted from Matsui 1993)

the proposed function can also well fit the measured deflection along the depth. The measured versus predicted pile head load-deflection relation, with or without adjusting the flexural rigidity of the pile in the analysis, is given in Fig. 7, in which neglecting variation of pile flexural rigidity tends to overestimate the pile capacity. The *p-y* curves obtained from the proposed method and from LPILE also show good agreement as illustrated in Fig. 8. Similar studies were also conducted for the PC pile P13 and the results are shown in Figs. 9–11. Reasonable agreement for the results of moment, shear force, and soil resistance obtained from the proposed method and from the computer program LPILE is also shown in Fig. 9. The importance of taking into account the effect of pile flexural rigidity in the analysis is also shown in the pile head load-deflection relationship of Fig. 10 and the *p-y* curves in Fig. 11.

Osaka Bay, Japan, Lateral Shaft Load Test

A full-scale lateral load test of two drilled shafts was conducted at Osaka Bay, Japan and was reported by Matsui (1993). Both shafts are 1.0 m in diameter and 25 m in length. The top 7 m of the test site consists of alluvial sandy soil overlying an alluvial clay soil layer of about 18 m thick. The shafts are supported on the diuvial sandy gravel layer underlying the clay layer. The elastic modulus

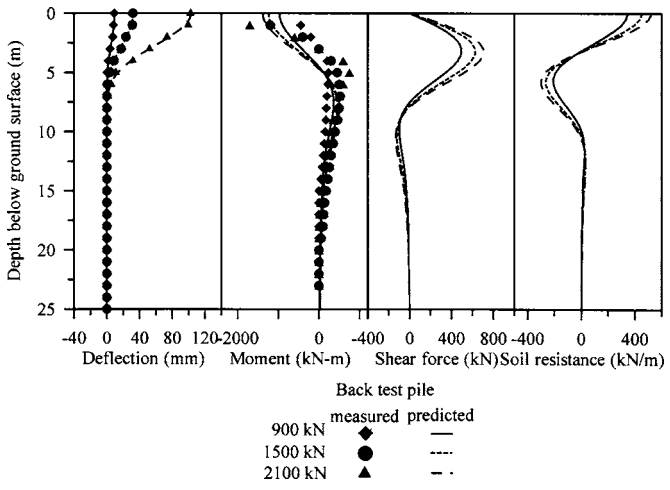

Fig. 13. Deflection, bending moment, shear force, and soil resistance distributions along the back pile shaft of Osaka Bay test pile

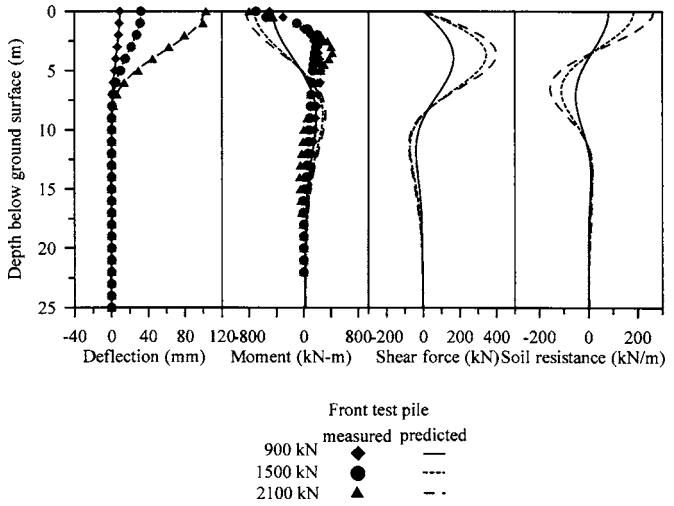

Fig. 14. Deflection, bending moment, shear force, and soil resistance distributions along the front pile shaft of Osaka Bay test pile

of the shaft is 3.0×10^7 kPa. The unconfined compressive strength of the concrete is 4.0×10^4 kPa. Inclinometers were installed along the shaft as shown in Fig. 12.

Lateral load with magnitude of 2.1 MN was applied at a connected beam, which was used to fix the heads of two shafts. Hence, case II boundary condition is assumed for both shafts to perform the analysis. Derived deflection, moment, shear, and soil resistance along the pile shaft versus embedded depth for back and front test shaft are shown in Figs. 13 and 14, respectively. As shown in the figures, pile group effect may have caused the difference on deflections, moments, and soil resistances of both shafts. The *p-y* curves obtained from the proposed method for back and front test shafts are also given in Figs. 15 and 16, respectively, for comparison.

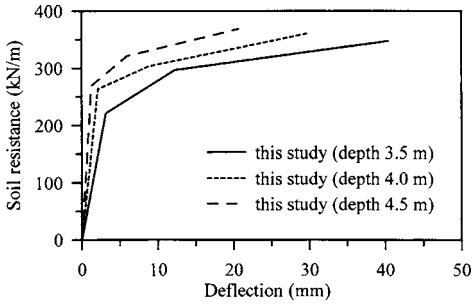

Fig. 15. *p-y* curves of back pile of Osaka Bay test pile

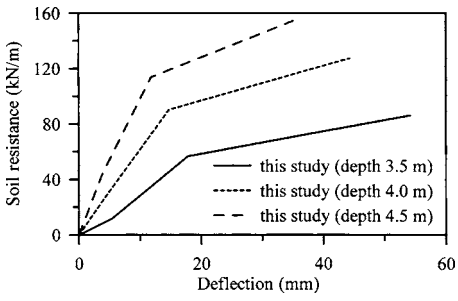

Fig. 16. *p-y* curves of front pile of Osaka Bay test pile

Summary and Conclusions

In this paper, a relatively simple method for interpreting lateral pile test results was proposed. Background theories, as well as detailed derivation of the proposed analytical method were described in this paper. Moreover, the feasibility of the developed method was further verified using results of three real case histories. Advantages of the proposed analytical method include: (1) only inclinometer data is needed for deriving the deflection function; (2) the derived deflection function can be used to describe lateral behaviors of a single pile system satisfying either free or fixed with sway pile head boundary conditions; and (3) nonlinear behavior for variation of the flexural rigidity of the pile is considered in the analysis and adjusted for each load increment.

It is necessary to point out that for short piles with high lateral loading, permanent lateral displacement might occur at the bottom of piles. Definitions of strain energy and potential energy used in this study need to be modified in order to establish the energy conservation relation for this case. Furthermore, energy conservation of the soil–pile system can no longer be included using only inclinometer data. Further study, is needed to develop analytical model for short pile applications.

Acknowledgments

This study was supported by the National Science Council, Taiwan, under Grant No. NSC 90-2211-E-019-023. Grateful appreciation is expressed for this support.

References

American Concrete Institute (ACI). (1995). "ACI building code requirements for structural concrete and commentary." *ACI 318-95*, Detroit.

Brown, D. A., Hidden, S. A., and Zhang, S. (1994). "Determination of *p-y* curves using inclinometer data." *Geotech. Test. J.*, 17(2), 150–158.

Chen, C. H. (1997). *"Data for planned pile group tests at Chiayi test site: Workshop report."* Dept. of Civil Engineering, National Taiwan Univ., Taipei, Taiwan.

Chen, J. T., Hong, H. K., Yeh, C. S., and Chyuan, S. W. (1996). "Integral representations and regularizations for a divergent series solution of a beam subjected to support motions." *Earthquake Eng. Struct. Dyn.*, 25(9), 909–925.

Han, J., and Frost, J. D. (2000). "Load-deflection response of transversely isotropic piles under lateral loads." *Int. J. Numer. Analyt. Meth. Geomech.*, 24(5), 509–529.

Hardy, G. H. (1994). *Divergent series*, Oxford University Press, Oxford, U.K.

Kramer, S. L. (1991). "Behavior of piles in full-scale field lateral loading tests." *Report No. WA-RD 215.1*, Washington State Dept. of Transportation, Va.

Matsui, T. (1993). "Case studies on cast-in-place bored piles and some considerations for design." *Deep foundation on bored and auger piles*, W. F. Van Impe, ed., Balkema, Rotterdam, The Netherlands, 77–101.

Ooi, P. S. K., and Ramsey, T. L. (2003). "Curvature and bending moments from inclinometer data." *Int. J. Geomech.*, 3(1), 64–74.

Pinto, P. L., Anderson, B., and Townsend, F. C. (1999). "Comparison of horizontal load transfer curves for laterally loaded piles form strain gages and slope inclinometer: A case study." *Field instrumentation for soil and rock*, *ASTM STP 1358*, G. N. Durham and W. A. Marr, eds., ASTM, West Conshohocken, Pa., 3–15.

Prakash, S., and Sharma, H. D. (1990). *Pile foundations in engineering practice*, Wiley, New York.

Reese, L. C., and Van Impe, W. F. (2001). *Single piles and pile groups under lateral loading*, Balkema, Rotterdam, The Netherlands, 121–123.

Reese, L. C., Wang, S. T., Isenhower, W. M., Arrellaga, J. A., and Hendrix, J. (2000). *Documentation of computer program LPILE Plus version 4.0 for Windows*, Ensoft, Inc., Austin, Tex.

Wang, J. T. S., and Lin, C. C. (1999). "A method for exact series solutions in structural mechanics." *J. Appl. Mech.*, 66(2), 380–387.

Wang, S. T., and Reese, L. C. (1991). "Analysis of piles under lateral load-computer program COM624P for the microcomputers." *Report No. FHwA-SA-91-002*, U.S. Dept. of Transportation, FHwA, Washington, D.C.